

# Lingbaoite, AgTe<sub>3</sub>, a new silver telluride from the Xiaoqinling gold district, central China

WEI JIAN<sup>1,\*</sup>, JINGWEN MAO<sup>1</sup>, BERND LEHMANN<sup>2</sup>, YANHE LI<sup>1</sup>, HUI SHOU YE<sup>1</sup>, JIANHUI CAI<sup>1</sup>, AND ZONGYAN LI<sup>3</sup>

<sup>1</sup>MNR Key Laboratory of Metallogeny and Mineral Assessment, Institute of Mineral Resources, Chinese Academy of Geological Sciences, Baiwanzhuang Street 26, Beijing, 100037, China

<sup>2</sup>Mineral Resources, Technische Universität Clausthal, Adolph-Roemer-Strasse 2A, Clausthal-Zellerfeld, 38678, Germany

<sup>3</sup>Jinyuan Mining Industry Co., Ltd, Jincheng Street 20, Lingbao 472500, China

## ABSTRACT

Lingbaoite, AgTe<sub>3</sub>, is a new silver telluride discovered in the S60 gold-bearing quartz vein, Xiaoqinling gold district, central China. The new mineral is named after Lingbao city, the municipality of which covers a major part of the Xiaoqinling gold district. Lingbaoite is only microscopically visible and occurs within pyrite as small composite inclusions (<50 μm) that commonly consist of lingbaoite, sylvanite, and chalcopyrite, and locally of bornite, galena, altaite, and stützite. The largest lingbaoite grain is about 30 × 12 μm in size. At least two stages of gold and telluride mineralization are recognized in the lingbaoite-bearing sample set. The first stage is characterized by the deposition of lingbaoite, native tellurium, and sylvanite, within the commonly observed mineral assemblages of lingbaoite + sylvanite + chalcopyrite and sylvanite + native tellurium + stützite. The second stage is characterized by the deposition of Bi-bearing minerals and native gold, within the commonly observed mineral assemblages of rucklidgeite + altaite + volynskite ± hessite ± petzite and rucklidgeite + gold ± altaite.

Lingbaoite is opaque and exhibits no internal reflections. In plane-polarized reflected light, lingbaoite shows a creamy yellow reflection color. The calculated density is 7.06 g/cm<sup>3</sup>. Seventeen WDS spot analyses from 17 different lingbaoite grains gave an empirical formula of Ag<sub>0.946</sub>Fe<sub>0.134</sub>Cu<sub>0.008</sub>Pb<sub>0.003</sub>Te<sub>2.841</sub>S<sub>0.067</sub>. When considering Ag and Te as the only two essential structural components, the empirical formula is Ag<sub>1.00</sub>Te<sub>3.00</sub>.

The EBSD and SAED data confirm the structural identity of lingbaoite and synthetic AgTe<sub>3</sub>. Synthetic AgTe<sub>3</sub> is trigonal, space group *R3m*, with *a* = 8.645 Å, *c* = 5.272 Å, *V* = 341.2 Å<sup>3</sup>, and *Z* = 3. The unit-cell parameters of lingbaoite are: *a* = 8.60 (5) Å, *c* = 5.40 (18) Å, *V* = 346 (9) Å<sup>3</sup>, and *Z* = 3. Synthetic AgTe<sub>3</sub>, and by analog lingbaoite, can be viewed as silver-stabilized cubic tellurium, which is an ordered (1:3 Ag:Te) analog of the α-polonium structure (i.e., simple cubic crystal structure). Synthetic AgTe<sub>3</sub> becomes a stable phase at above 0.4 GPa, but can also occur in a metastable state at atmospheric pressure.

Lingbaoite probably formed through the cooling of polymetallic melt droplets within the hydrothermal system. Lingbaoite and associated minerals (e.g., sylvanite, native tellurium) reveal a previously unrecognized but perhaps common magmatic-hydrothermal process in the Xiaoqinling gold district, which precedes the precipitation of native gold, suggesting that gold mineralization in the Xiaoqinling gold district involves multiple superimposed processes of gold enrichment.

**Keywords:** Lingbaoite, AgTe<sub>3</sub>, new mineral, silver telluride, polymetallic melt, magmatic-hydrothermal origin

## INTRODUCTION

The compound AgTe<sub>3</sub> was first recognized in nature as fine-grained mineral inclusions in pyrite from the S60 gold-bearing quartz vein, Xiaoqinling gold district, central China (Jian et al. 2014). Further investigation of the AgTe<sub>3</sub> grains from the same sample set confirms the structural identity of lingbaoite and synthetic AgTe<sub>3</sub> (Range et al. 1982). The mineral and the mineral name were approved by the Commission on New Minerals, Nomenclature and Classification of the International Mineral-

ogical Association (Application 2018-138). The new mineral is named after Lingbao city, which is about 30 km northeast of the mine where the new mineral was discovered. The municipality of Lingbao constitutes a major part of the Xiaoqinling gold district, which is the second-largest gold production area in China. Holotype material is deposited in the collections of the Geological Museum of China, Beijing, China, catalog number M13812.

## OCCURRENCE AND ASSOCIATED MINERALS

Lingbaoite was discovered as abundant micrometer-sized grains in gold ore samples collected underground from the S60 gold-bearing quartz vein (34°23'N, 110°34'E), which

\* E-mail: weijian851@gmail.com

is about 30 km southwest of Lingbao city, Henan province, central China.

The Xiaoqinling gold district is located at the southern margin of the North China Craton and belongs to the Qinling-Dabie Orogen. The strata exposed in the Xiaoqinling gold district are dominated by Archean amphibolite-facies metamorphic rocks (e.g., biotite plagiogneiss, amphibolite gneiss, amphibolite, quartzite, and marble: Cai and Su 1985) of the Taihua Group, which hosts most of the gold-bearing quartz veins. The Archean rocks were intruded by Paleoproterozoic pegmatite (Li, H.M. et al. 2007), Proterozoic and Mesozoic granitic intrusions (Wang et al. 2010; Ding et al. 2011; Hu et al. 2012; Zhao et al. 2012), and Paleoproterozoic and Early Cretaceous mafic dikes (Wang et al. 2008; Zhao et al. 2010; Bi et al. 2011a).

The Xiaoqinling gold district represents the second-largest gold production area in China and has a proven gold reserve of more than 630 tonnes (Jian et al. 2015), with more than 1200 gold-bearing quartz veins documented (Li et al. 1996; Mao et al. 2002). The gold-bearing quartz veins show a very pronounced Te signature (Bi et al. 2011b; Jian et al. 2014, 2015, 2018). Tellurium concentration in the gold ores is typically in the range of tens to hundreds of parts per million (Luan et al. 1985; Xue et al. 2004). The S60 gold-bearing quartz vein, with estimated gold resources of about 100 tonnes (average Au grade ~10 g/t), represents one of the largest gold-bearing quartz veins in the Xiaoqinling gold district (Figure 1).

Abundant micrometer-sized grains of lingbaoite were observed in polished sections prepared from gold ores. Other min-

erals observed in the polished sections include quartz, sulfides (pyrite, chalcopyrite, bornite, sphalerite, and galena), tellurides (altaite, stützite, hessite, sylvanite, petzite, calaverite, rucklidgeite, volynskite, and buckhornite), Bi-sulfosalts (wittichenite and an unnamed phase  $\text{Cu}_{20}\text{FePb}_{11}\text{Bi}_9\text{S}_{37}$ ), as well as native gold and tellurium (Figs. 2 and 3).

At least two stages of gold and telluride mineralization are recognized in the lingbaoite-bearing sample set. The first stage (I) is in the form of mineral inclusions in pyrite, with the commonly observed mineral assemblages of lingbaoite + sylvanite + chalcopyrite and sylvanite + native tellurium + stützite. Lingbaoite, for example, occurs within pyrite as small composite inclusions (<50  $\mu\text{m}$ ), which commonly consist of lingbaoite, sylvanite, and chalcopyrite, and locally of bornite, galena, altaite, and stützite (Figs. 2 and 3). Lingbaoite and native tellurium often occur in adjacent composite inclusions (Fig. 2d), but they have not been found to coexist in the same composite inclusion.

The second stage (II) is characterized by the deposition of Bi-bearing minerals (i.e., rucklidgeite, volynskite) and native gold. They occur in the two commonly observed mineral assemblages: rucklidgeite + altaite + volynskite  $\pm$  hessite  $\pm$  petzite (e.g., Fig. 3d) and rucklidgeite + gold  $\pm$  altaite (Fig. 3c). These mineral assemblages occur as larger patches connecting with fractures or as fracture fillings in pyrite (Fig. 3), contrasting with the lingbaoite-bearing assemblages, which occur as mineral inclusions in pyrite. Trails of lingbaoite-bearing inclusions are also cut by fractures filled by assemblages of Bi-bearing minerals (Fig. 3e) and native gold (Fig. 3b).

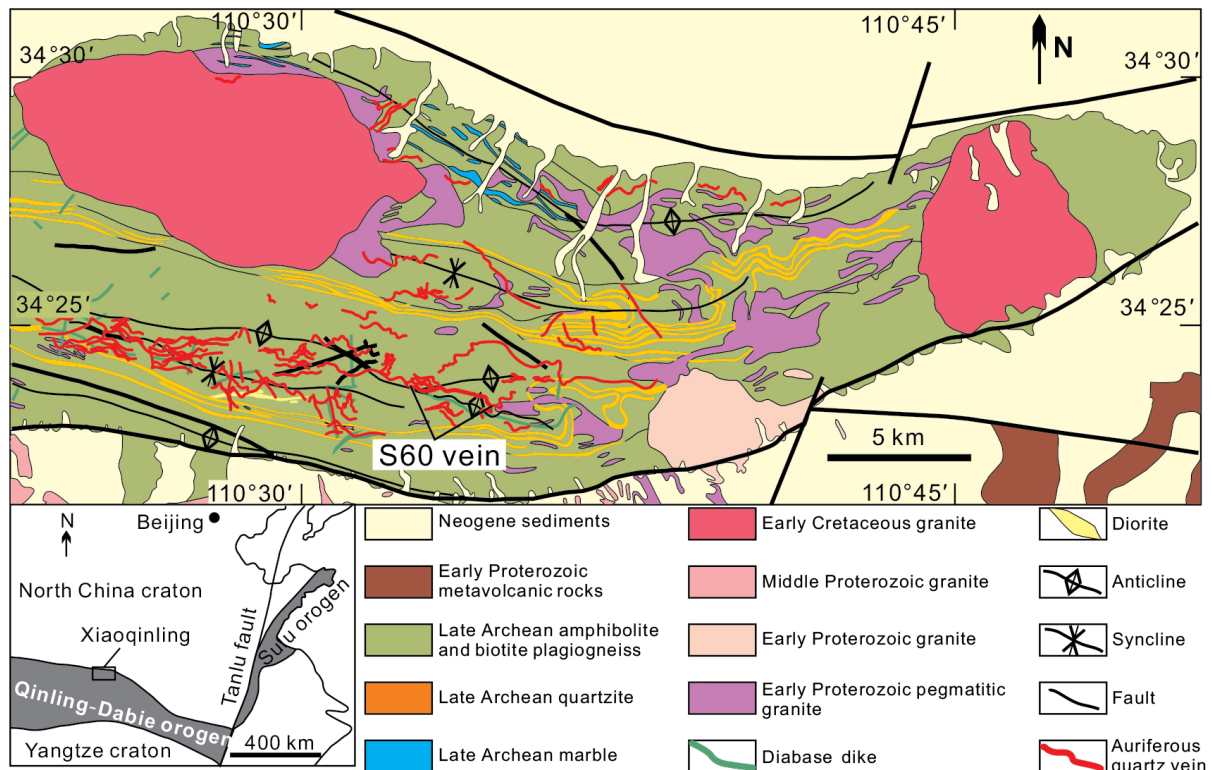
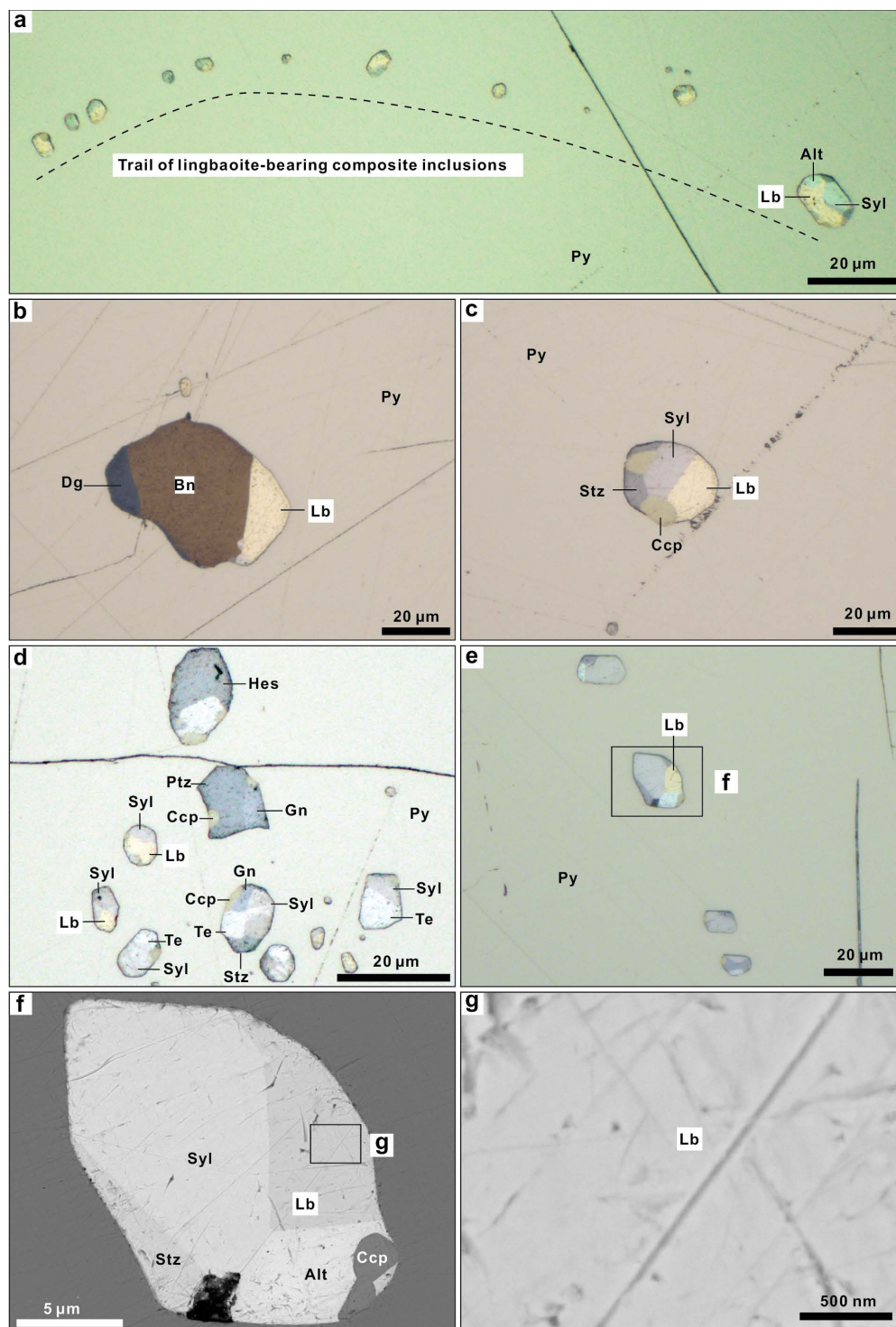
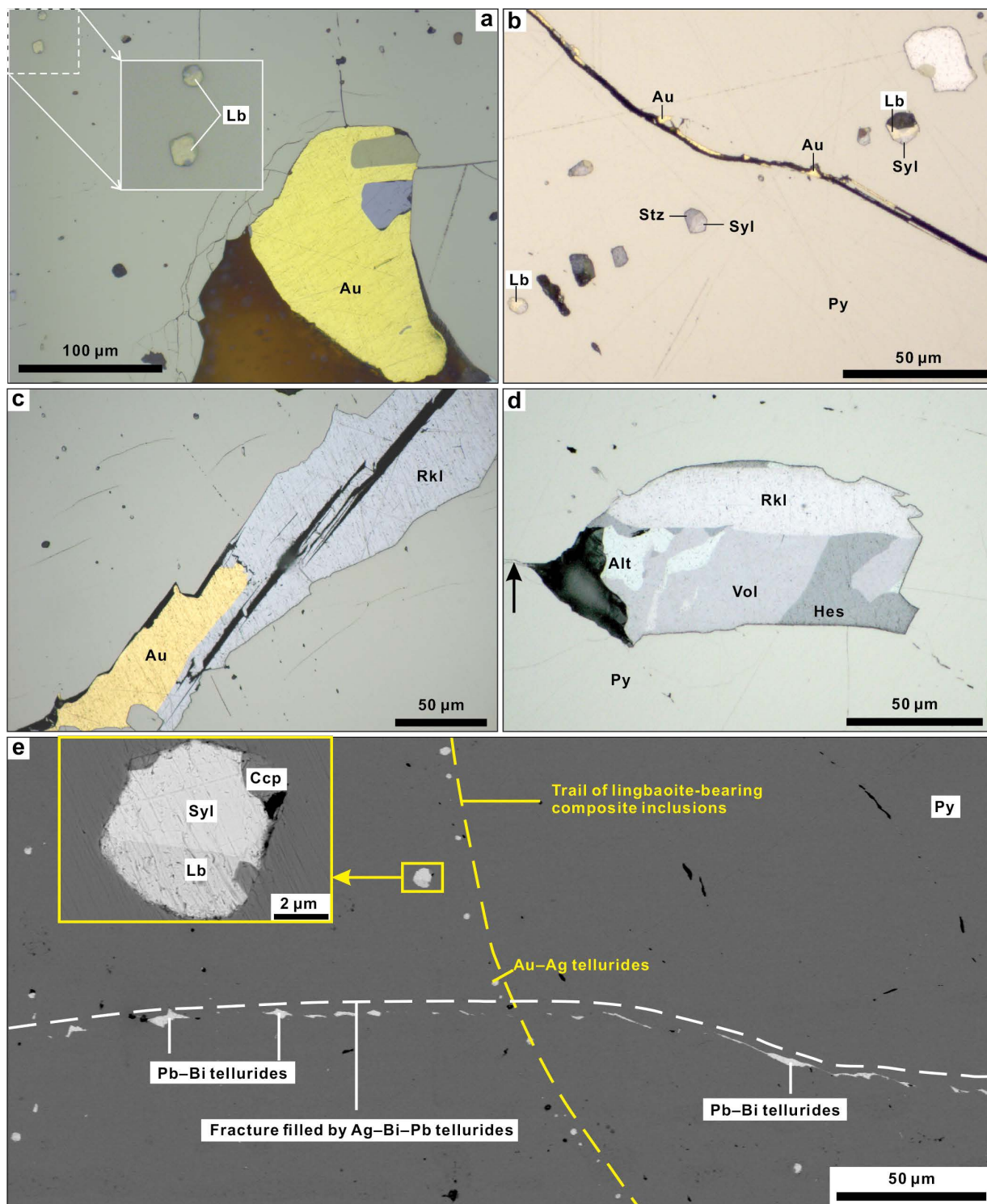


FIGURE 1. Geologic map of the Xiaoqinling gold district and its position in China (after Jian et al. 2014).



**FIGURE 2.** Photomicrographs (a–e, plane-polarized reflected light, oil immersion) and SEM images (f–g) of lingbaoite and associated minerals (stage I). (a) Trail of lingbaoite-bearing composite inclusions in pyrite. The largest composite inclusion in the right consists of lingbaoite, sylvanite, altaite, and other small, unidentified phases. (b) Composite inclusion consisting of lingbaoite, bornite, and digenite. (c) Composite inclusion consisting of lingbaoite, chalcopyrite, sylvanite, and stützite. (d) Lingbaoite-bearing composite inclusions and native tellurium-bearing composite inclusions in pyrite (from Jian et al. 2014). (e) Composite inclusion consisting of lingbaoite, sylvanite, chalcopyrite, and stützite, detailed in f. (f) Close-up view of the composite inclusion indicated in e. (g) Close-up view of a part of the lingbaoite grain indicated in f. Note lingbaoite is compositionally homogeneous. Abbreviations: Alt = altaite, Au = gold, Bn = bornite, Cp = chalcopyrite, Dg = digenite, Gn = galena, Lb = lingbaoite, Ptz = petzite, Py = pyrite, Stz = stützite, Syl = sylvanite, Te = native tellurium.





**FIGURE 3.** Photomicrographs (a–d, plane-polarized reflected light, oil immersion) and SEM image (e) of stage II tellurides, native gold, and their cross-cut relation to lingbaoite. (a) Gold, galena, and chalcopyrite in pyrite fracture. Note two small lingbaoite grains (top left) have reflection color similar to gold but are slightly darker than gold. (b) Trail of lingbaoite-bearing composite inclusions cut by a fracture filled by gold (from Jian et al. 2014). (c) Gold and rucklidgeite in pyrite fracture. (d) Aggregate of rucklidgeite + altaite + volynskite + hessite in pyrite. Note that the left margin of the aggregate is delineated by a micro-fracture (arrow). (e) Trail of lingbaoite-bearing composite inclusions cut by a fracture filled by Ag–Bi–Pb telluride minerals (modified from Jian et al. 2014). Abbreviations: Alt = altaite, Au = gold, Cp = chalcopyrite, Gn = galena, Hes = hessite, Lb = lingbaoite, Py = pyrite, Rkl = rucklidgeite, Syl = sylvanite, Vol = volynskite.

**PHYSICAL AND OPTICAL PROPERTIES**

Lingbaoite is only microscopically visible and occurs within pyrite as small composite inclusions (<50 μm). The largest lingbaoite grain is about 30 × 12 μm in size (Fig. 2b). Despite its small grain size, lingbaoite is widespread in the polished sections. Color (megascopic), streak, hardness, tenacity, cleavage, fracture, and density could not be determined because of the small grain size. The calculated density is 7.06 g/cm<sup>3</sup> based on the empirical formula of AgTe<sub>3</sub> and the cell parameters of lingbaoite.

This mineral is opaque and exhibits no internal reflections. In plane-polarized reflected light, lingbaoite shows a creamy yellow reflection color, without discernable reflectance pleochroism or anisotropy, similar to the reflection color of native gold but with lower reflectance (Figs. 3a and 3b).

Reflectance values of lingbaoite were measured in air using a CRAIC 20/30 PV microspectrophotometer at Southern University of Science and Technology, China. The reference material is Al with MgF<sub>2</sub> coating. Although the used reference material is not an approved Commission on Ore Mineralogy of the International Mineralogical Association standard, the calibration of this reference material is traceable to NIST/NRC. The reflectance values were obtained from five spots in three different lingbaoite grains from two polished sections, with ×100 objective and 1.1 × 1.1 μm aperture size. Reflectance data are given in Table 1 and Figure 4.

**CHEMICAL COMPOSITION**

Electron microprobe data for lingbaoite were reported in a previous study (Jian et al. 2014) and are cited below. Electron microprobe analysis was carried out at Clausthal University of Technology, Germany, using a Cameca SX100 electron microprobe. Preliminary qualitative analyses by energy-dispersive X-ray spectrometry (EDS) revealed the presence of only four elements: Te, Ag, Fe, and S. Quantitative chemical analyses were obtained by wavelength-dispersive X-ray spectrometry (WDS), operated at 20 kV and 20 nA, with beam diameter of 1 μm. The X-ray emission lines used were: SKα, FeKα, CuKα, AgLα, TeLα, AuLα, PbMα, and BiMα. The count times for peak and background were: 10 and 5 s for SKα, 14 and 7 s for FeKα, 14 and 7 s for CuKα, 18 and 9 s for AgLα, 12 and 6 s for TeLα, 20 and 10 s for AuLα, 16 and 8 s for PbMα, and 10 and 5 s for BiMα. The detection limits for the measured elements are as follows: 0.05–0.07 wt% S, 0.24–0.30 wt% Bi, 0.15–0.17 wt% Ag, 0.26–0.49 wt% Au, 0.12–0.13 wt% Cu, 0.21–0.24 wt% Te, 0.06–0.07 wt% Fe, 0.23–0.31 wt% Pb. Results of 17 WDS spot analyses from 17 different lingbaoite grains are summarized,

**TABLE 1.** Reflectance values for lingbaoite

λ (nm)	R <sub>max</sub> (%)	R <sub>min</sub> (%)	λ (nm)	R <sub>max</sub> (%)	R <sub>min</sub> (%)
400	26.2	22.4	560	51.6	45.8
420	28.3	26.7	580	53.0	47.5
440	33.4	30.4	<b>589</b>	<b>53.6</b>	<b>48.2</b>
460	38.1	34.0	600	54.0	48.8
<b>470</b>	<b>39.9</b>	<b>35.6</b>	620	55.0	50.2
480	41.8	37.0	640	55.7	51.3
500	45.0	39.6	<b>650</b>	<b>55.9</b>	<b>51.7</b>
520	47.7	41.9	660	56.2	52.1
540	49.8	44.0	680	56.6	53.0
<b>546</b>	<b>50.3</b>	<b>44.5</b>	700	57.0	53.3

Notes: The reflectance values were obtained from five spots in three different lingbaoite grains.

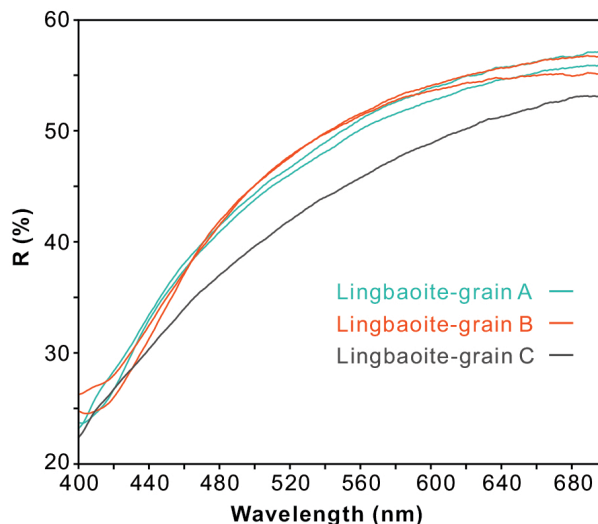


**FIGURE 4.** Reflectance data for lingbaoite in air. The reflectance values (R%) are plotted vs. wavelength in nm. The data were obtained from five spots in three different lingbaoite grains.

together with the standards used, in Table 2.

All the analyzed lingbaoite grains contain small amounts of Fe (1.04–1.97 wt%) and S (0.12–0.85 wt%), and some lingbaoite grains also contain trace amounts of Cu (0.1–0.6 wt%). A contribution to these Fe, Cu, and S concentrations is probably caused by contamination by adjacent sulfide minerals. This is because lingbaoite grains are small and always occur as inclusions in pyrite. Indeed, seven out of eight lingbaoite grains containing Cu are in assemblages with chalcopyrite and/or bornite. Lead was only detected in two grains, while Au and Bi are always below minimum detection limits.

The mean empirical formula is Ag<sub>0.946</sub>Fe<sub>0.134</sub>Cu<sub>0.008</sub>Pb<sub>0.003</sub>Te<sub>2.841</sub>S<sub>0.067</sub>, assuming that the measured Fe, Cu, and Pb contents are real. When considering Ag and Te as the only two essential structural components, the empirical formula of lingbaoite ranges between Ag<sub>0.99</sub>Te<sub>3.01</sub> and Ag<sub>1.03</sub>Te<sub>2.97</sub>, average Ag<sub>1.00</sub>Te<sub>3.00</sub>. The ideal formula is AgTe<sub>3</sub>, which requires Ag 21.98, Te 78.02, total 100 wt%.

**CRYSTALLOGRAPHY**

The small grain size of lingbaoite prevented investigations by means of X-ray diffraction. Instead, electron backscattered diffraction (EBSD) and selected-area electron diffraction (SAED) were carried out for the crystallographic characterization.

**Electron backscattered diffraction**

EBSD analyses were performed at the State Key Laboratory for Advanced Metals and Materials at University of Science and

**TABLE 2.** Chemical data (in wt%) for lingbaoite

Constituent	Mean	Range	St. dev.	Reference material
S	0.45	0.12–0.85	0.29	Natural pyrite
Ag	21.34	20.83–22.00	0.33	Ag, pure metal
Cu	0.11	0–0.62	0.16	Cu, pure metal
Te	75.81	74.79–76.73	0.59	Synthetic PbTe
Fe	1.57	1.04–1.97	0.26	Natural pyrite
Pb	0.14	0–2.20	0.51	Synthetic PbTe
Total	99.43	98.11–100.20		



Technology, Beijing, using a ZEISS SUPRA55 Field Emission Scanning Electron Microscope equipped with a NordlysMax3 EBSD system for collecting Kikuchi bands and Aztec software for data interpretation. The analytical parameters were as follows: accelerating voltage = 20 kV, magnification = 2500~10 000, working distance = 14~21 mm, tilt angle = 70.00°.

The center of eight Kikuchi bands for lingbaoite was automatically detected using the Aztec software. The solid angles calculated from the patterns were compared with synthetic AgTe<sub>3</sub> to index the patterns. The EBSD patterns obtained from eight different lingbaoite grains were found to match the patterns generated from the structure of synthetic AgTe<sub>3</sub> (Fig. 5). The values of the mean angular deviation (MAD, i.e., goodness of fit of the solution) between the calculated and measured Kikuchi bands are between 0.33° and 0.79°. These values reveal a very good match; as long as values of mean angular deviation are less than 1°, they are considered as indicators of an acceptable fit (Vymazalová et al. 2009, 2012).

### Transmission electron microscopy

A TEM foil of about 150 nm thickness was prepared on a FEI focused ion beam (FIB)-SEM platform at the GeoForschungs-Zentrum (GFZ) in Potsdam, Germany. Details on TEM foil

preparation can be found in Wirth (2004, 2009). The TEM foil consists mainly of a lingbaoite grain and its surrounding pyrite. Images of the foil and its location in polished section before cutting are shown in Figure 6. Selected-area electron diffraction (SAED) analyses for lingbaoite were carried out using a JEM-2100 (HR) Transmission Electron Microscope equipped with a double-tilt holder, a Gatan digital camera, and an INCA Energy TEM100 energy-dispersive spectroscopy instrument at the Institute of Mineral Resources, Chinese Academy of Geological Sciences, and operated at 200 kV. The SAED patterns of lingbaoite (Fig. 7) were taken from the circled area in the TEM foil (Fig. 6d) and from seven different zone axes.

Based on the obtained SAED patterns of lingbaoite, we measured the interplanar spacing values for lingbaoite. These values are in excellent agreement with the measured *d*-spacings for synthetic AgTe<sub>3</sub>, with the absolute value of difference less than 0.02 Å (Supplemental<sup>1</sup> Table S1). We also measured the angles between adjacent planes in the SAED patterns of lingbaoite. The measured angles of lingbaoite agree well with the calculated angles of synthetic AgTe<sub>3</sub>, with the absolute value of difference less than 1.1° (Supplemental<sup>1</sup> Table S2). Therefore, the excellent agreement of the *d*-spacings and plane angles of

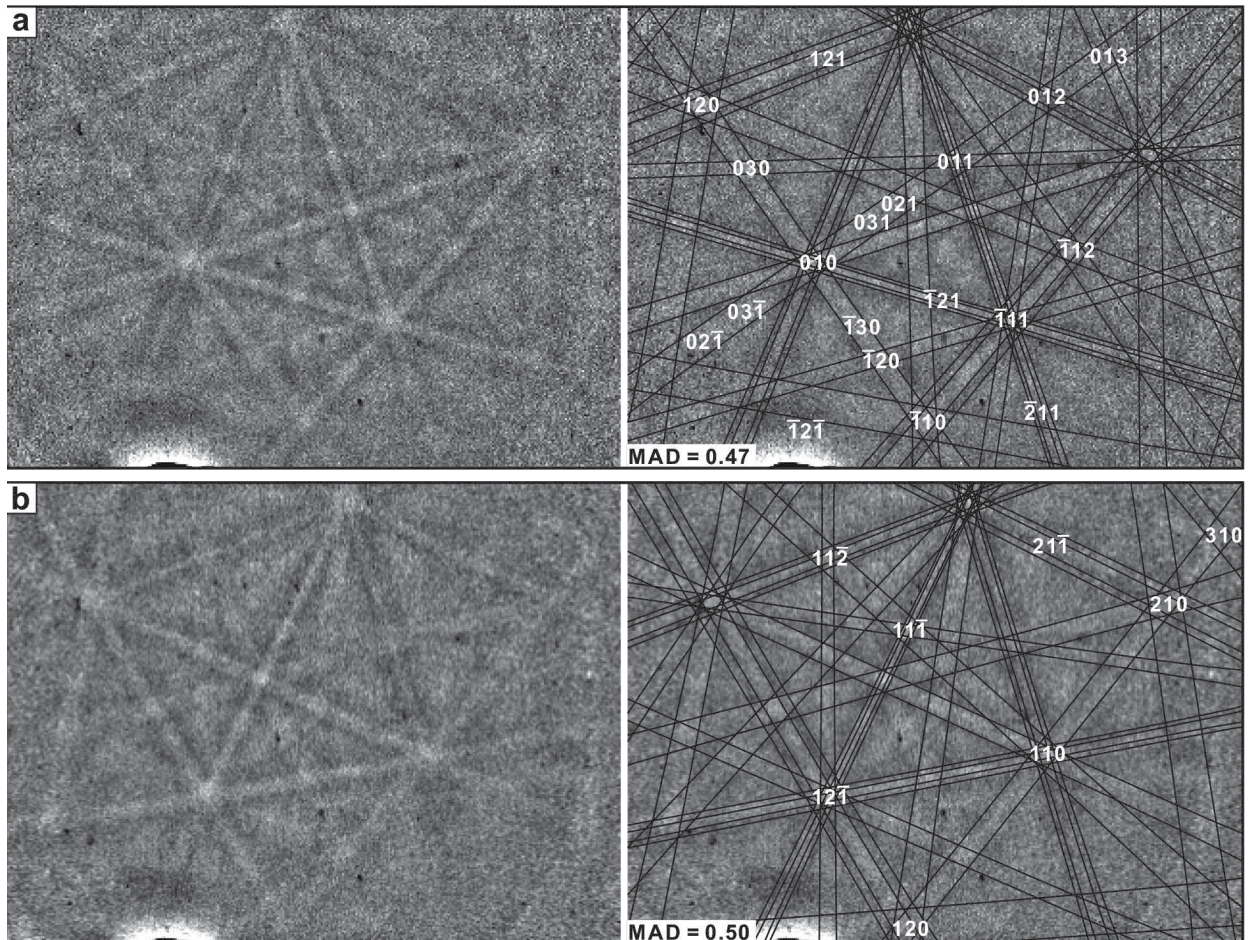


**FIGURE 5.** EBSD images of two natural lingbaoite grains. The Kikuchi bands and the values of the mean angular deviation (MAD) are indicated in the right column.

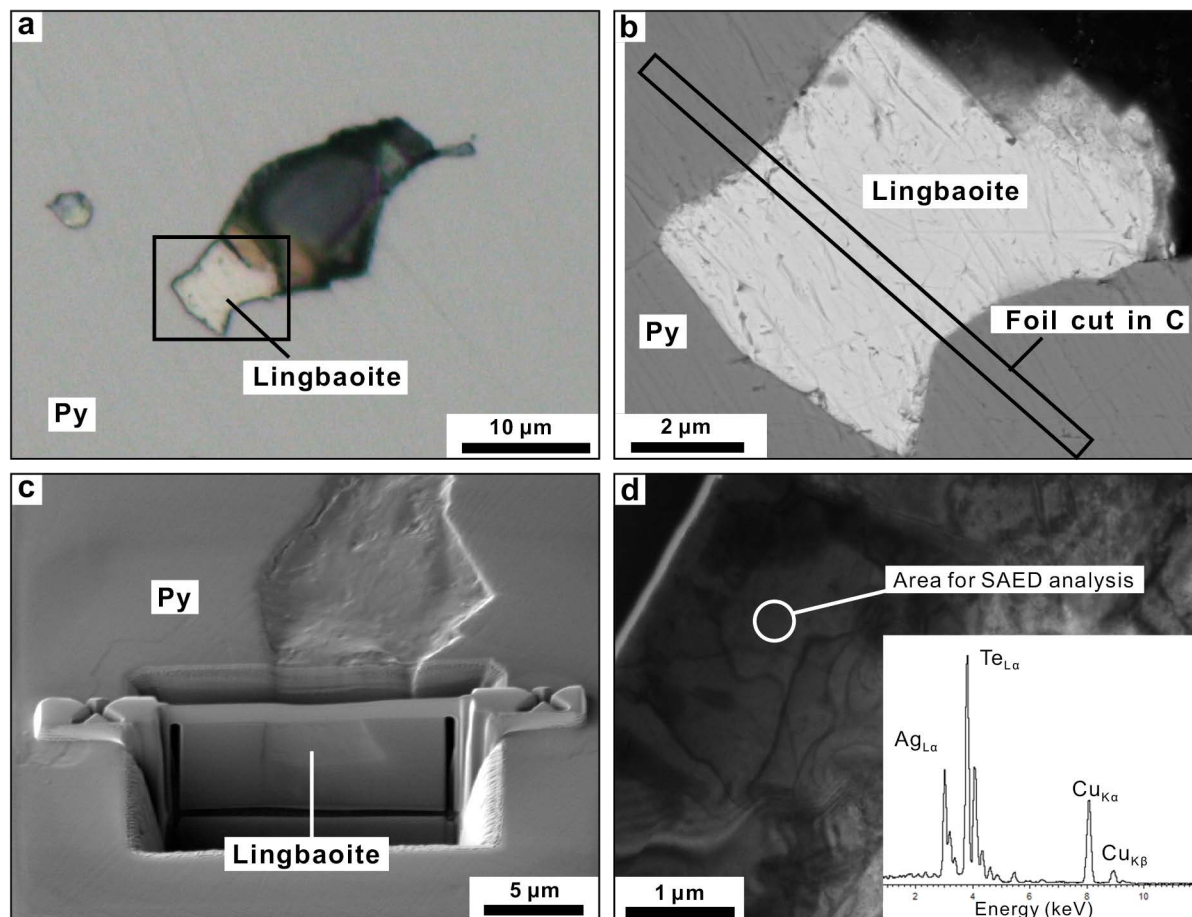


**FIGURE 6.** Images of the TEM foil for SAED analysis and its location in polished section before cutting. (a) Photomicrograph (plane-polarized reflected light, oil immersion) showing lingbaoite occurs as mineral inclusion in pyrite. (b) SEM image showing a close-up view of the rectangular area indicated in a, with the location of the TEM foil to be cut indicated. (c) SEM image of the TEM foil extracted from the area indicated in b. (d) Bright-field TEM image showing a part of the TEM foil with the position for SAED analysis indicated (circled area) and the TEM-EDS spectra (inset) for the circled area (lingbaoite). The peaks for Cu are caused by the TEM Cu-grid.

lingbaoite with those for synthetic AgTe<sub>3</sub>, confirms the structural identity of lingbaoite and synthetic AgTe<sub>3</sub>.

#### Unit-cell parameters

The unit-cell parameters of lingbaoite are calculated based on the interplanar spacing values measured through the obtained SAED patterns. Lingbaoite belongs to the trigonal crystal system and *R3m* space group. The calculated unit-cell parameters of lingbaoite are as follows:  $a = 8.60(5) \text{ \AA}$ ,  $c = 5.40(18) \text{ \AA}$ ,  $V = 346(9) \text{ \AA}^3$ , and  $Z = 3$ . The EBSD and SAED data confirm the structural identity of lingbaoite and synthetic AgTe<sub>3</sub>. Therefore, the unit-cell parameters of synthetic AgTe<sub>3</sub> (Range et al. 1982) are also cited here:  $a = 8.645 \text{ \AA}$ ,  $c = 5.272 \text{ \AA}$ ,  $V = 341.2 \text{ \AA}^3$ , and  $Z = 3$ . X-ray powder diffraction data were calculated from the data on the crystal structure of the synthetic equivalent, AgTe<sub>3</sub> (Range et al. 1982), and are given in Supplemental<sup>1</sup> Table S1, along with the measured interplanar spacing data for lingbaoite.

#### Crystal structure

AgTe<sub>3</sub>, the synthetic equivalent of lingbaoite, belongs to the trigonal crystal system. The crystal structure of synthetic AgTe<sub>3</sub>

(Range et al. 1982) is best interpreted in terms of an inner-centered, pseudocubic ( $\alpha = 90.15^\circ$ ) arrangement of the rhombohedral unit cell. In this arrangement, the Ag atoms occupy the center and corners, while the Te atoms occupy the face- and edge-centers of a cube. Thus the crystal structure of AgTe<sub>3</sub> can be regarded as an ordered (1:3 Ag:Te) analog of the  $\alpha$ -polonium structure (i.e., simple cubic crystal structure). Silver is octahedrally coordinated by Te [Ag–Te:  $3 \times 302.2(5)$ ,  $3 \times 308.3(5)$  pm], each Te in turn being surrounded by a square arrangement of four further Te atoms together with two Ag atoms to give a Te(Te<sub>4</sub>Ag<sub>2</sub>) octahedron [distances:  $4 \times \text{Te–Te } 305.2(5)$ ,  $1 \times \text{Ag–Te } 302.2(5)$ ,  $1 \times \text{Ag–Te } 308.3(5)$  pm]. The Te–Te distances in the three-dimensional array of Te atoms are close to the value of 302 pm postulated for metallic tellurium with  $\alpha$ -polonium structure (von Hippel 1948); the valence angles at Te are almost  $90^\circ$  (89.79, 89.84,  $90.52^\circ$ ). The electron energy loss spectroscopy (EELS) spectrum and valence-electron density of AgTe<sub>3</sub> are similar to those of Te (Stander and Range 1983). These similarities, together with the metallic luster and metallic conductivity [ $\rho(300 \text{ K}) = 1 \times 10^{-6} \text{ \Omega}\cdot\text{m}$ ] of AgTe<sub>3</sub>, strongly support the idea that AgTe<sub>3</sub> can be viewed as silver-stabilized cubic tellurium (Range et al. 1982).



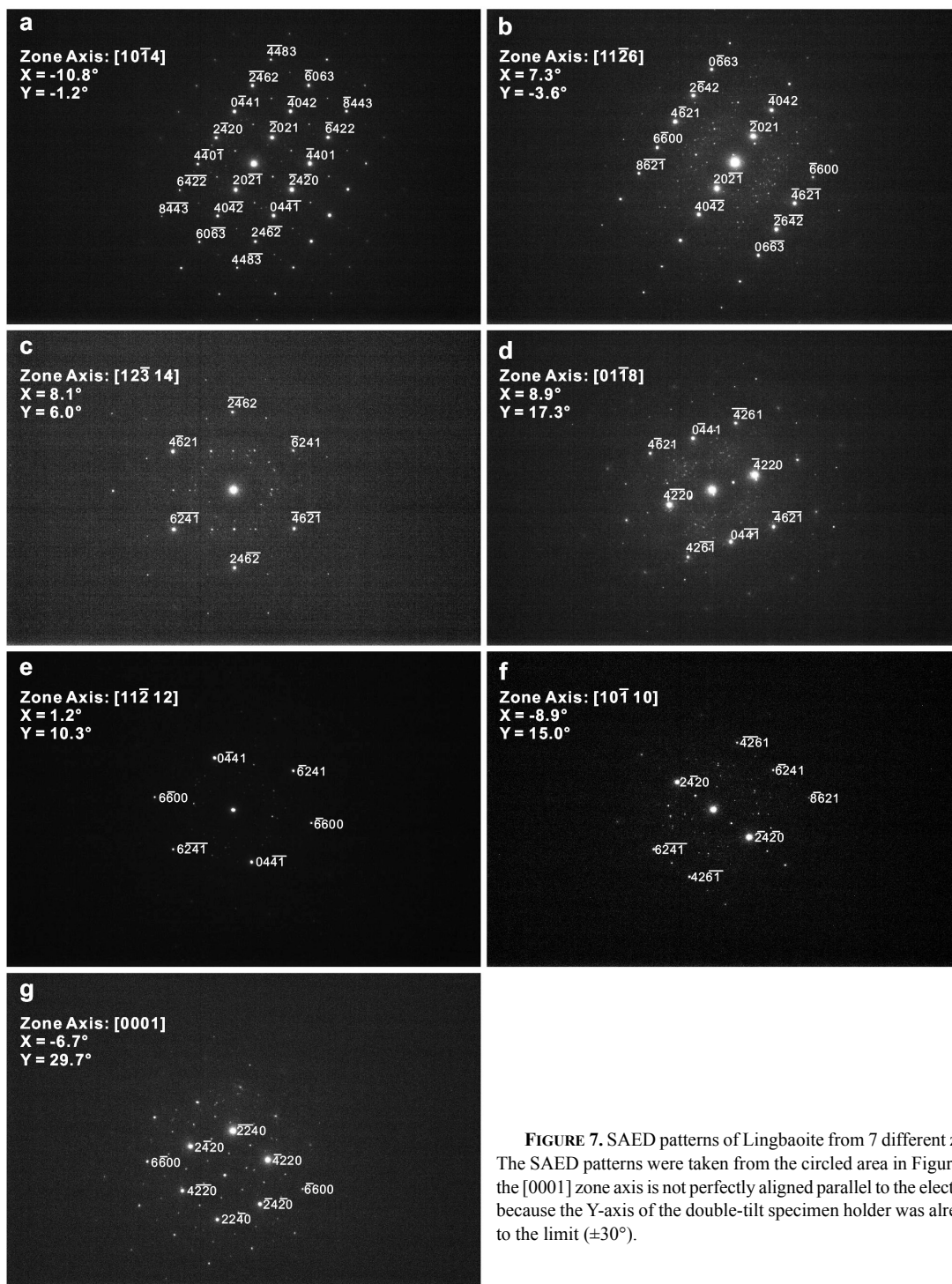


**FIGURE 7.** SAED patterns of Lingbaoite from 7 different zone axes. The SAED patterns were taken from the circled area in Figure 6d. In g, the [0001] zone axis is not perfectly aligned parallel to the electron beam, because the Y-axis of the double-tilt specimen holder was already tilted to the limit ( $\pm 30^\circ$ ).

The crystal structure of synthetic  $\text{AgTe}_3$  is shown in Figure 8. The Wyckoff positions, atom coordinates, and bond distances for synthetic  $\text{AgTe}_3$  are shown in Tables 3 and 4.

#### Relation to other species

Minerals and synthetic phases chemically or structurally related to lingbaoite are shown in Table 5. Structurally, lingbaoite is closely

related to the  $\alpha$ -polonium structure, a simple cubic crystal structure with  $a = 3.359 \text{ \AA}$ . Chemically, lingbaoite ( $\text{AgTe}_3$ ) is a new member of the silver telluride minerals; the other three silver telluride minerals are hessite ( $\text{Ag}_2\text{Te}$ ), stützite ( $\text{Ag}_{5-x}\text{Te}_3$ ), and empressite ( $\text{AgTe}$ ). Lingbaoite, however, clearly differs from the other silver tellurides by its much higher tellurium content (75 at% Te), as well as its creamy yellow reflection color and its crystal structure.



## DISCUSSION

The experimental study of Range and Thomas (1983) shows that synthetic AgTe<sub>3</sub> becomes a stable phase at above 0.4 GPa (Fig. 9) and converts into a mixture of Ag<sub>3-x</sub>Te<sub>3</sub> and Te at lower pressures. However, synthetic AgTe<sub>3</sub> can also occur in a metastable state at lower pressures. For example, AgTe<sub>3</sub> was successfully produced at atmospheric pressure through rapid quenching of Te-Ag melt (75 at% Te) from >365 °C, and retransformation of this phase required high-temperature annealing (Range and Thomas 1983). The high-pressure AgTe<sub>3</sub> and metastable AgTe<sub>3</sub> obtained at atmospheric pressure are identical (Range and Thomas 1983).

We speculate that lingbaoite either (1) formed at above 0.4 GPa (i.e. >15 km depth); or (2) formed at lower pressures through rapid cooling of polymetallic melt. The first mechanism, however, seems unlikely. First, the quartz vein hosting lingbaoite is a large vein system that is 0.3 to 7 m in width and extends for more than 4 km along strike (Li et al. 1996), suggesting the vein was emplaced in a brittle environment (i.e., less than 10–15 km depth: Sibson 1986). Second, a formation depth of 15 km would suggest a temperature of 375–450 °C for the ambient rocks (assuming a geothermal gradient of 25–30 °C km<sup>-1</sup>), surpassing the expected formation temperature of lingbaoite and associated minerals. According to the experimental studies of Cabri (1965), sylvanite melts at 354 °C and the intergrowth assemblage native tellurium + sylvanite + stützite (Fig. 2d) suggests a formation temperature of less than 330 °C.

Therefore, it appears more likely that lingbaoite formed through cooling of polymetallic melt at lower pressures. The mineral assemblages present in the lingbaoite-bearing composite inclusions

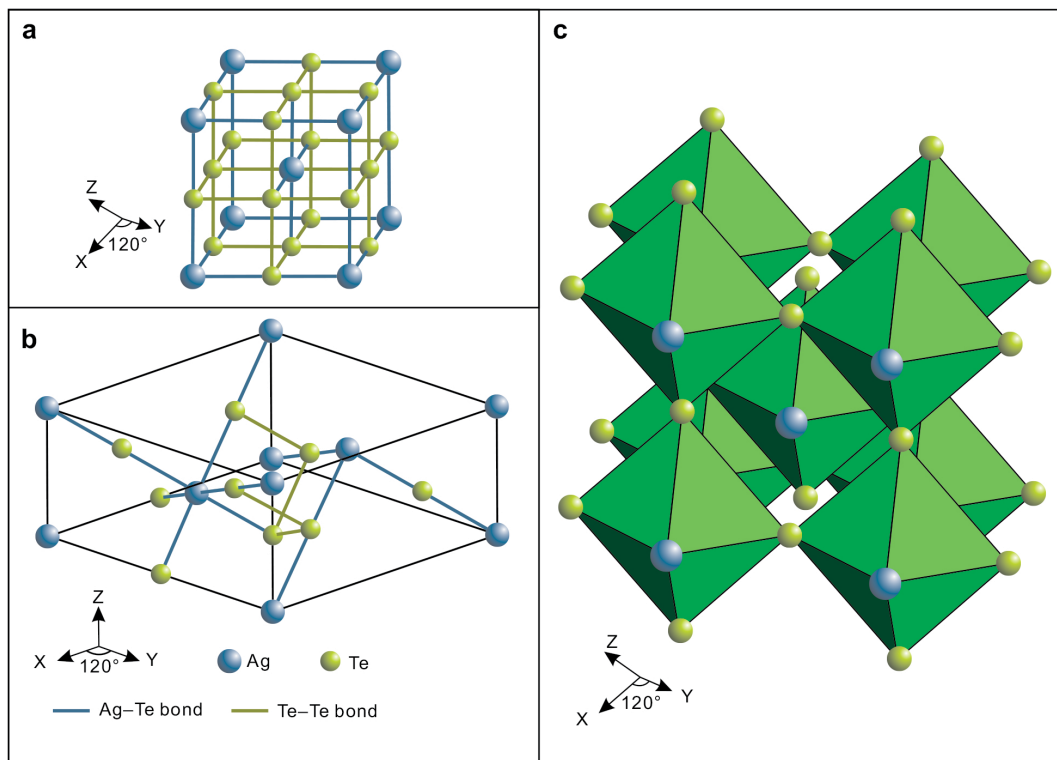
**TABLE 3.** Wyckoff positions and atom coordinates for synthetic AgTe<sub>3</sub> (from Range et al. 1982)

Atom	Site	x	y	z
Ag	3a	0	0	0
Te	9b	0.1672	-0.1672	0.3412

**TABLE 4.** Bond distances (Å) for synthetic AgTe<sub>3</sub> within one Te(Te<sub>4</sub>Ag<sub>2</sub>) octahedron (from Range et al. 1982)

Atom 1	Atom 2	Distance
Te	Te	3.052(5)×4
Ag	Te	3.022(5)×1
Ag	Te	3.083(5)×1

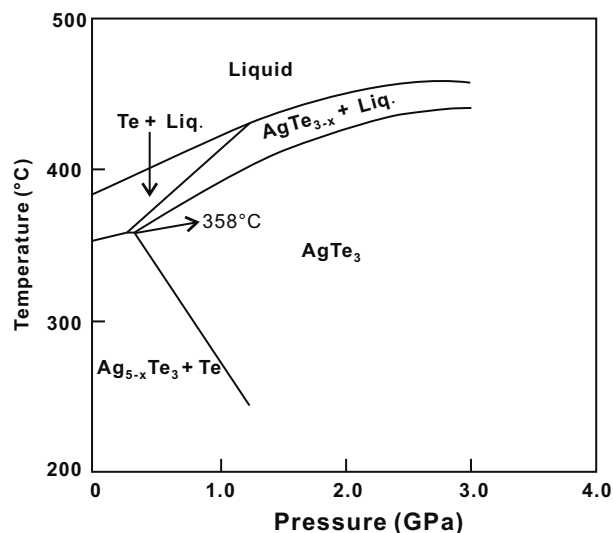
(Figs. 2 and 3) indicate a complex Au-Ag-Te-Fe-Cu-Pb-S system. Although it is impossible to tell at which temperature such a complex system would melt, we speculate that the minimum melting temperature for such a system will be lower than 304 °C. This is because melts can exist in the Au-Ag-Te system down to 304 °C (Cabri 1965), and additional elements will drive melting points lower in most chemical systems (Frost et al. 2002; Cook et al. 2009). It is unclear how the polymetallic melt precipitating lingbaoite formed, but it has been experimentally proved that Bi-dominated melts can form directly from hydrothermal fluids through reduction of Bi<sup>3+</sup> (Tooth et al. 2011), and the presence of polymetallic melts has been proposed in a wide variety of hydrothermal gold deposit (e.g., Frost et al. 2002; Cook and Ciobanu 2004; Ciobanu et al. 2006; Cook et al. 2009; Cockerton and Tomkins 2012; Zhou et al. 2017). Bismuth and bismuth-tellurium melt inclusions have also been observed recently in quartz-cassiterite veins (Guimarães et al. 2019).



**FIGURE 8.** Crystal structure of AgTe<sub>3</sub>, the synthetic equivalent of lingbaoite. (a) Pseudocubic structure (modified from Range et al. 1982). (b) The unit cell of AgTe<sub>3</sub>. The solid black lines outline a single unit cell. (c) Arrangement of the Te(Te<sub>4</sub>Ag<sub>2</sub>) octahedron (modified from Range et al. 1982).

**TABLE 5.** Minerals and phases chemically/structurally related to lingbaoite

Mineral/Phase	Formula	Crystal system	Space group	Cell parameters				Reference	
				a (Å)	b (Å)	c (Å)	Z cell angle		
Hessite	Ag <sub>2</sub> Te	Monoclinic	P2 <sub>1</sub> /C	8.162	4.467	8.973	4	β = 124.15°	Schneider and Schulz (1993)
Stützite	Ag <sub>5-x</sub> Te <sub>3</sub>	Hexagonal	C6/mmm	13.380		8.450	7		Honea (1964)
Synthetic AgTe <sub>3</sub>	AgTe <sub>3</sub>	Trigonal	R3m	8.645		5.272	3	γ = 120°	Range et al. (1982)
Lingbaoite	AgTe <sub>3</sub>	AgTe <sub>3</sub>	R3m	8.60		5.40	3	γ = 120°	This study
Empressite	AgTe	Orthorhombic	Pnma	8.882	20.100	4.614	16		Bindi et al. (2004)
Native silver	Ag	Cubic	Fm3m	4.086			4		Novgorodova et al. (1981)
Native tellurium	Te	Trigonal	P3 <sub>2</sub> 1	4.447		5.915	3	γ = 120°	Wyckoff (1963)
α-polonium	Po	Cubic	Pm3m	3.345			1		Beamer and Maxwell (1949)
Simple cubic tellurium (hypothetical phase)	Te	Cubic	Pm3m	3.020			1		von Hippel (1948)

**FIGURE 9.** *P-T* phase relations in the silver-tellurium system at 75 at% Te (modified from Range and Thomas 1983).

### IMPLICATIONS

Lingbaoite and associated sylvanite reveal a previously unrecognized but perhaps common gold enrichment process in the Xiaoqinling gold district, preceding the precipitation of native gold and Bi-bearing minerals. This further suggests that gold mineralization in the Xiaoqinling gold district involves multiple gold enrichment processes, which seem essential for the formation of large deposits (e.g., Large et al. 2007; Meffre et al. 2016; Fougereuse et al. 2017; Kerr et al. 2018).

This study also reveals a magmatic affinity of the hydrothermal system. The fluid responsible for the deposition of lingbaoite and associated minerals is characterized by high sulfur and tellurium fugacity with no bismuth, as evidenced by the presence of lingbaoite, native tellurium, sylvanite, bornite, as well as the absence of native gold and Bi-bearing minerals. High sulfur and tellurium fugacity of the fluid implies a magmatic-hydrothermal origin of the hydrothermal system (e.g., Afifi et al. 1988; Einaudi et al. 2003). Minerals such as native tellurium and bornite, for example, commonly occur in magmatic-hydrothermal systems, such as porphyry Cu-Au-Mo (Einaudi et al. 2003; Cook et al. 2011) and epithermal Au deposits (Afifi et al. 1988). Biotite and sericite <sup>40</sup>Ar/<sup>39</sup>Ar age data indicate that gold mineralization in the S60 vein took place in the Early Cretaceous (134.5–123.7 Ma; Li et al. 2012a). Although causative intrusions have not been discovered, the early gold mineralization event in the S60 vein

is likely related to the large-scale Early Cretaceous magmatism (e.g., alkaline granites and A-type granites; Ye et al. 2008; Zhou et al. 2008; Mao et al. 2010) in the Xiaoqinling gold district and adjacent areas, in relation to lithospheric thinning, asthenospheric upwelling, and partial melting of the lower crust and upper mantle in eastern China (Mao et al. 2008, 2010; Li et al. 2012a, 2012b; Zhao et al. 2019).

### ACKNOWLEDGMENTS

Ulf Hemmerling is greatly thanked for preparing excellent polished sections. Richard Wirth and Anja Schreiber are thanked for the preparation of TEM foils. Hong Yu is greatly acknowledged for SAED data acquisition and interpretation. Xu Tang is also thanked for the interpretation of SAED data. Jianping He is thanked for carrying out the EBSD measurements. Zhijian Niu and Ingmar Ratschinski are thanked for their assistance with the SEM analysis. Junlong Yan is thanked for providing access to the Microspectrophotometer. Zhiqiang Cui is thanked for providing some ore samples. Alexandre Raphael Cabral, Anna Vymazalová, Xiaoxia Wang, He Rong, Guowu Li, Yuan Xue, and Lin Li are thanked for their constructive suggestions on how to propose a new mineral. Chairman Ritsuro Miyawaki and members of IMA-CNMMN are thanked for their comments on the new-mineral proposal submitted for approval by the commission. Constructive reviews by Degao Zhai, Nigel Cook, and Christopher J. Stanley considerably improved the paper and are greatly acknowledged. Aaron Celestian is especially thanked for the editorial handling.

### FUNDING

This research was jointly funded by the National Natural Science Foundation of China (41602039), Research Grant of the Chinese Academy of Geological Sciences (K1605, YK1702), and the Geological Survey Project of China (DD20190368).

### REFERENCES CITED

- Afifi, A.M., Kelly, W.C., and Essene, E.J. (1988) Phase relations among tellurides, sulfides, and oxides: II Applications to telluride-bearing ore deposits. *Economic Geology*, 83, 395–404.
- Beamer, W.H., and Maxwell, C.R. (1949) Physical properties of polonium. II. X-ray studies and crystal structure. *Journal of Chemical Physics*, 17, 1293–1298.
- Bi, S.J., Li, J.W., and Li, Z.K. (2011a) Geological significance and geochronology of Paleoproterozoic mafic dykes of Xiaoqinling gold district, southern margin of the North China craton. *Earth Science—Journal of China University of Geosciences*, 36, 17–32 (in Chinese with English abstract).
- Bi, S.J., Li, J.W., Zhou, M.F., and Li, Z.K. (2011b) Gold distribution in As deficient pyrite and telluride mineralogy of the Yangzhaiyu gold deposit, Xiaoqinling district, southern North China craton. *Mineralium Deposita*, 46, 925–941.
- Bindi, L., Spry, P.G., and Cipriani, C. (2004) Empressite, AgTe, from the Empress-Josephine Mine, Colorado, USA: composition, physical properties and determination of the crystal structure. *American Mineralogist*, 89, 1043–1047.
- Cabri, L.J. (1965) Phase relations in the Au-Ag-Te systems and their mineralogical significance. *Economic Geology*, 60, 1569–1606.
- Cai, N.Z., and Su, Z.B. (1985) Stratigraphic subdivision and distinction of primary rock-types of the Taihua Group in the Xiaoqinling Mountain. *Regional Geology of China*, 13, 35–44 (in Chinese with English abstract).
- Ciobanu, C.L., Cook, N.J., Damian, F., and Damian, G. (2006) Gold scavenged by bismuth melts: An example from Alpine shear-remobilized in the Highis, Massif, Romania. *Mineralogy and Petrology*, 87, 351–384.
- Cockerton, A.B.D., and Tomkins, A.G. (2012) Insights into the liquid bismuth collector model through analysis of the Bi-Au Stormont skarn prospect, northwest Tasmania. *Economic Geology*, 107, 667–682.
- Cook, N.J., and Ciobanu, C.L. (2004) Bismuth tellurides and sulphosalts from the Larga hydrothermal system, Metaliferi Mts., Romania: Paragenesis and genetic significance. *Mineralogical Magazine*, 68, 301–321.
- Cook, N.J., Ciobanu, C.L., and Mao, J. (2009) Textural control on gold distribution

- in As-free pyrite from the Dongping, Huangtuliang and Hougou gold deposits, North China Craton (Hebei Province, China). *Chemical Geology*, 264, 101–121.
- Cook, N.J., Ciobanu, C.L., Danyushevsky, L.V., and Gilbert, S. (2011) Minor and trace elements in bornite and associated Cu-(Fe)-sulfides: A LA-ICP-MS study: *Geochimica et Cosmochimica Acta*, 75, 6473–6496.
- Ding, L.X., Ma, C.Q., Li, J.W., Robinson, P.T., Deng, X.D., Zhang, C., and Xu, W.C. (2011) Timing and genesis of the adakitic and shoshonitic intrusions in the Laonishan complex, southern margin of the North China craton: Implications for post-collisional magmatism associated with the Qinling orogeny. *Lithos*, 126, 212–232.
- Einaudi, M.T., Hedenquist, J., and Inan, E. (2003) Sulfidation state of fluids in active and extinct hydrothermal systems: Transitions from porphyry to epithermal environments. In S.F. Simmons and I. Graham, Eds., *Volcanic, Geothermal, and Ore-Forming Fluids: Rulers and Witnesses of Processes within the Earth*, p 285–313. Society of Economic Geologists Special Publication 10 Volume, Society of Economic Geologists, USA.
- Fougerouse, D., Micklethwaite, S., Ulrich, S., Miller, J., Godel, B., Adams, D.T., and McCuaig, T.C. (2017) Evidence for two stages of mineralization in West Africa's largest gold deposit, Obuasi, Ghana. *Economic Geology*, 112, 3–22.
- Frost, B.R., Mavrogenes, J.A., and Tomkins, A.G. (2002) Partial melting of sulfide ore deposits during medium- and high-grade metamorphism. *Canadian Mineralogist*, 40, 1–18.
- Guimarães, F.S., Cabral, A.R., Lehmann, B., Rio, F.J., Ávila, M.A.B., Castro, M.P., and Queiroga, G.N. (2019) Bismuth-melt trails trapped in cassiterite-quartz veins. *Terra Nova*, 00, 1–8.
- Honea, R.M. (1964) Empressite and stützite redefined. *American Mineralogist*, 49, 325–338.
- Hu, J., Jiang, S.Y., Zhao, H.X., Shao, Y., Zhang, Z.Z., Xiao, E., Wang, Y.F., Dai, B.Z., and Li, H.Y. (2012) Geochemistry and petrogenesis of the Huashan granites and their implications for the Mesozoic tectonic settings in the Xiaolinling gold mineralization belt, NW China. *Journal of Asian Earth Science*, 56, 276–289.
- Jian, W., Lehmann, B., Mao, J.W., Ye, H.S., Li, Z.Y., Zhang, J.G., Zhang, H., Feng, J.W., and Ye, Y.Z. (2014) Telluride and Bi-sulfosalt mineralogy of the Yangzhaiyu gold deposit, Xiaolinling region, central China. *Canadian Mineralogist*, 52, 883–898.
- Jian, W., Lehmann, B., Mao, J.W., Ye, H.S., Li, Z.Y., He, H.J., Zhang, J.G., Zhang, H., and Feng, J.W. (2015) Mineralogy, fluid characteristics, and Re-Os age of the Late Triassic Dahu Au-Mo deposit, Xiaolinling region, central China: Evidence for a magmatic-hydrothermal origin. *Economic Geology*, 110, 119–145.
- Jian, W., Albrecht, M., Lehmann, B., Mao, J.W., Horn, I., Li, Y.H., Ye, H.S., Li, Z.Y., Fang, G.G., and Xue, Y.S. (2018) UV-fs-LA-ICP-MS Analysis of CO<sub>2</sub>-rich Fluid Inclusions in a Frozen State: Example from the Dahu Au-Mo Deposit, Xiaolinling Region, Central China. *Geofluids* 2018, 1–17, Article ID 3692180, doi:10.1155/2018/3692180.
- Kerr, M.J., Hanley, J.J., Kontak, D.J., Morrison, G.G., Petrus, J., Fayek, M., and Zajacz, Z. (2018) Evidence of upgrading of gold tenor in an orogenic quartz-carbonate vein system by late magmatic-hydrothermal fluids at the Madrid Deposit, Hope Bay Greenstone Belt, Nunavut, Canada. *Geochimica et Cosmochimica Acta*, 241, 180–218.
- Large, R.R., Maslennikov, V.V., Robert, F., Danyushevsky, L.V., and Chang, Z.S. (2007) Multistage sedimentary and metamorphic origin of pyrite and gold in the giant Sukhoi log deposit, Lena Gold province, Russia. *Economic Geology*, 102, 1233–1267.
- Li, S.M., Qu, L.Q., Su, Z.B., Huang, J.J., Wang, X.S., and Yue, Z.S. (1996) The geology and metallogenic prediction of the gold deposit in Xiaolinling, 250 p., Geological Publishing House, Beijing (in Chinese with English abstract).
- Li, H.M., Chen, Y.C., Wang, D.H., Ye, H.S., Wang, Y.B., Zhang, C.Q., and Dai, J.Z. (2007) SHRIMP U-Pb ages of metamorphic rocks and veins in the Xiaolinling area, and their geological significance. *Acta Petrologica Sinica*, 23, 2504–2512 (in Chinese with English abstract).
- Li, J.W., Li, Z.K., Zhou, M.F., Chen, L., Bi, S.J., Deng, X.D., Qiu, H.N., Cohen, B., Seibly, D., and Zhao, X.F. (2012a) The Early Cretaceous Yangzhaiyu lode gold deposit, North China Craton: A link between craton reactivation and gold veining. *Economic Geology*, 107, 43–79.
- Li, J.W., Bi, S.J., Seibly, D., Chen, L., Vasconcelos, P., Thiede, D., Zhou, M.F., Zhao, X.F., Li, Z.K., and Qiu, H.N. (2012b) Giant Mesozoic gold provinces related to the destruction of the North China craton. *Earth and Planetary Science Letters*, 349–350, 26–37.
- Luan, S.W., Cao, D.C., Fang, Y.K., and Wang, J.Y. (1985) Geochemistry of Xiaolinling gold deposits. *Minerals and Rocks*, 5, 1–118 (in Chinese with English abstract).
- Mao, J.W., Goldfarb, R.J., Zhang, Z.W., Xu, W.Y., Qiu, Y.M., and Deng, J. (2002) Gold deposits in the Xiaolinling-Xiong'er shan region, Qinling Mountains, central China. *Mineralium Deposita*, 37, 306–325.
- Mao, J.W., Xie, G.Q., Bierlein, F., Qu, W.J., Du, A.D., Ye, H.S., Pirajno, F., Li, H.M., Guo, B.J., Li, Y.F., and Yang, Z.Q. (2008) Tectonic implications from Re-Os dating of Mesozoic molybdenum deposits in the East Qinling-Dabie orogenic belt. *Geochimica et Cosmochimica Acta*, 72, 4607–4626.
- Mao, J.W., Xie, G.Q., Pirajno, F., Ye, H.S., Wang, Y.B., Li, Y.F., Xiang, J.F., and Zhao, H.J. (2010) Late Jurassic-Early Cretaceous granitoid magmatism in eastern Qinling, central-eastern China: SHRIMP zircon U-Pb ages and tectonic implications. *Australian Journal of Earth Sciences*, 57, 51–78.
- Meffre, S., Large, R.R., Steadman, J.A., Gregory, D.D., Stepanov, A.S., Kamenetsky, V.S., Ehrig, K., and Scott, R.J. (2016) Multi-stage enrichment processes for large gold-bearing ore deposits. *Ore Geology Reviews*, 76, 268–279.
- Novgorodova, M.I., Gorshkov, A.I., and Mokhov, A.V. (1981) Native silver and its new structural modifications. *International Geology Review*, 23, 485–494.
- Range, K.J., and Thomas, M. (1983) Pressure-temperature relations in the silver-tellurium system at 75 at-% tellurium. *Materials Research Bulletin*, 18, 1195–1202.
- Range, K.J., Zabel, M., Rau, F., Krziwanek, F.V., Marx, R., and Panzer, B. (1982) A novel three-dimensional tellurium array: high-pressure synthesis and crystal structure of AgTe<sub>3</sub>. *Angewandte Chemie*, 21, 706–707.
- Schneider, J., and Schulz, H. (1993) X-ray powder diffraction of Ag<sub>2</sub>Te at temperatures up to 1123 K. *Zeitschrift für Kristallographie*, 203, 1–15.
- Sibson, R.H. (1986) Brecciation processes in fault zones: Inferences from earthquake rupturing. *Pure and Applied Geophysics*, 124, 159–175.
- Stander, C.M., and Range, K.J. (1983) Determination of valence-electron concentration in AgTe<sub>3</sub> by electron energy loss spectroscopy. *Solid State Communications*, 47, 843–844.
- Tooth, B., Ciobanu, C.L., Green, L., O'Neill, B., and Brugger, J. (2011) Bi-melt formation and gold scavenging from hydrothermal fluids: An experimental study. *Geochimica et Cosmochimica Acta*, 75, 5423–5443.
- Wang, T.H., Mao, J.W., and Wang, Y.B. (2008) Research on SHRIMP U-Pb chronology in Xiaolinling-Xiong'er shan area: The evidence of delamination of lithosphere in Qinling orogenic belt. *Acta Petrologica Sinica*, 24, 1273–1287 (in Chinese with English abstract).
- Wang, Y.T., Ye, H.S., Ye, A.W., Sun, Y., Li, Y.G., and Zhang, C.Q. (2010) Zircon SHRIMP U-Pb ages and their significances of the Wenyu and Niangniangshan granitic plutons in the Xiaolinling area, central China. *Chinese Journal of Geology*, 45, 167–180 (in Chinese with English abstract).
- Wirth, R. (2004) Focused Ion Beam (FIB): a novel technology for advanced application of micro- and nanoanalysis in geosciences and applied mineralogy. *European Journal of Mineralogy*, 16, 863–876.
- (2009) Focused Ion Beam (FIB) combined with SEM and TEM: Advanced analytical tools for studies of chemical composition, microstructure and crystal structure in biomaterials on a nanometre scale. *Chemical Geology*, 261, 217–229.
- Wyckoff, R.W.G. (1963) *Crystal Structures I*, 2nd ed., 467 p. Interscience Publishers, New York.
- von Hippel, A. (1948) Structure and conductivity in the VI<sub>6</sub> group of the periodic system. *The Journal of Chemical Physics*, 16, 372–380.
- Vymazalová, A., Laufek, F., Drábek, M., Haloda, J., Sidorinova, T., and Plasil, J. Pasavaite, Pd<sub>2</sub>Pb<sub>2</sub>Te<sub>2</sub>, a new platinum-group mineral species from Norilsk-Talnakh Ni-Cu camp, Russia. *Canadian Mineralogist*, 47, 53–62, 2009.
- Vymazalová, A., Laufek, F., Drábek, M., Cabral, A.R., Haloda, J., Sidorinová, T., Lehmann, B., Galbiatti, H.F., and Drahoukoupil, J. Jacutingaite, Pt<sub>2</sub>HgSe<sub>3</sub>, a new platinum-group mineral from the Cauê iron-ore deposit, Itabira district, Minas Gerais, Brazil. *Canadian Mineralogist*, 50, 431–440, 2012.
- Xue, L.W., Chai, S.G., Zhu, J.W., and Li, M.L. (2004) Study on accompanying tellurium resources in Xiaolinling gold deposit. *Conservation and Utilization of Mineral Resources*, 42–45 (in Chinese with English abstract).
- Ye, H.S., Mao, J.W., Xu, L.G., Gao, J.J., Xie, G.Q., Li, X.Q., and He, C.F. (2008) SHRIMP zircon U-Pb dating and geochemistry of the Taishanmiaojiao aluminous A-type granite in western Henan Province. *Geological Review*, 54, 1–13 (in Chinese with English abstract).
- Zhao, H.J., Mao, J.W., Ye, H.S., Xie, G.Q., and Yang, Z.X. (2010) Geochronology and geochemistry of the alkaline granite porphyry and diabase dikes in Huanglongpu area of Shanxi Province: Petrogenesis and implications for tectonic environment. *Geology of China*, 37, 12–27 (in Chinese with English abstract).
- Zhao, H.X., Jiang, S.H., Frimmel, H.E., Dai, B.Z., and Ma, L. (2012) Geochemistry, geochronology and Sr-Nd-Hf isotopes of two Mesozoic granitoids in the Xiaolinling gold district: Implication for large-scale lithospheric thinning in the North China craton. *Chemical Geology*, 294–295, 173–189.
- Zhao, X.F., Li, Z.K., Zhao, S.R., Bi, S.J., and Li, J.W. (2019) Early Cretaceous Regional Scale Magmatic Hydrothermal Metallogenic System at the Southern Margin of the North China Craton. *Earth Science*, 44, 52–68 (in Chinese with English abstract).
- Zhou, H.S., Ma, C.Q., Zhang, C., Chen, L., Zhang, J.Y., and She, Z.B. (2008) Yanshanian aluminous A-type granitoids in the Chunshui of Biyang, south margin of North China Craton: Implications from petrology, geochronology and geochemistry. *Acta Petrologica Sinica*, 24, 49–64 (in Chinese with English abstract).
- Zhou, H., Sun, X., Cook, N.J., Lin, H., Fu, Y., Zhong, R., and Brugger, J. (2017) Nano-to micron-scale particulate gold hosted by magnetite: a product of gold scavenging by bismuth melts. *Economic Geology*, 112, 993–1010.

MANUSCRIPT RECEIVED JUNE 20, 2019

MANUSCRIPT ACCEPTED NOVEMBER 26, 2019

MANUSCRIPT HANDLED BY AARON CELESTIAN

## Endnote:

<sup>1</sup>Deposit item AM-20-57167, Supplemental Tables. Deposit items are free to all readers and found on the MSA website, via the specific issue's Table of Contents (go to [http://www.minsocam.org/MSA/AmMin/TOC/2020/May2020\\_data/May2020\\_data.html](http://www.minsocam.org/MSA/AmMin/TOC/2020/May2020_data/May2020_data.html)).